Supporting Information

A Conjoined Rectilinear Collision Cell and Pulsed Extraction Ion Trap with Auxiliary DC Electrodes.

Hamish Stewart*, Dmitry Grinfeld, Alexander Wagner, Alexander Kholomeev, Matthias Biel, Anastassios Giannakopulos, Alexander Makarov and Christian Hock

Thermo Fisher Scientific, 11 Hannah-Kunath Str., 28199 Bremen, Germany.

Email: hamish.stewart@thermofisher.com

Supplementary Images of Ion Processor

Figure S1 shows photographs of the complete Ion Processor device, including how the PCB covers serve to close the cell and the PCB-based entrance lens.

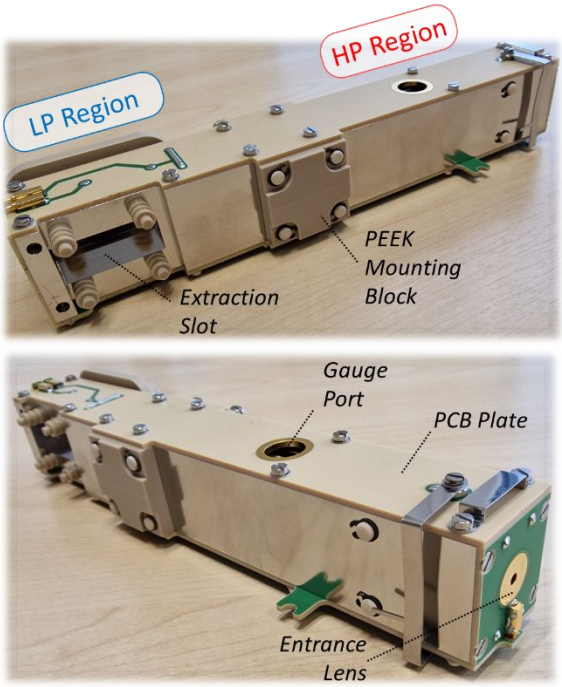

Figure S1. Photographs of prototype Ion Processor

Second Generation Improvements

The design reported in this publication involves very high mechanical accuracy on largely wire eroded parts, as well as large numbers of custom spacers in addition to electrodes. It was also found to be easy for the very thin negative auxiliary DC trapping electrode to bend slightly. An altered design that improves reproducible accuracy is

shown in Figure S2. The auxiliary trapping electrode was remade as a small part glued to the more substantial positive electrode via a ceramic mounting piece. This gave the electrode much better support and reduced the need for rods and spacers in the overall assembly. In addition, the remaining stack of RF and DC electrodes in each region were, instead of being individually wire eroded and assembled, were part eroded, glued together on rods, and the final erosion stage made on the complete stack. This removed a potentially difficult tolerance chain from the device, without altering function. The PCB-based entrance lens was also replaced by a thin stainless steel plate design, which appeared to be easier to tune for transmission, and immune to metallization failures that can occur with ion optics based on PCB.

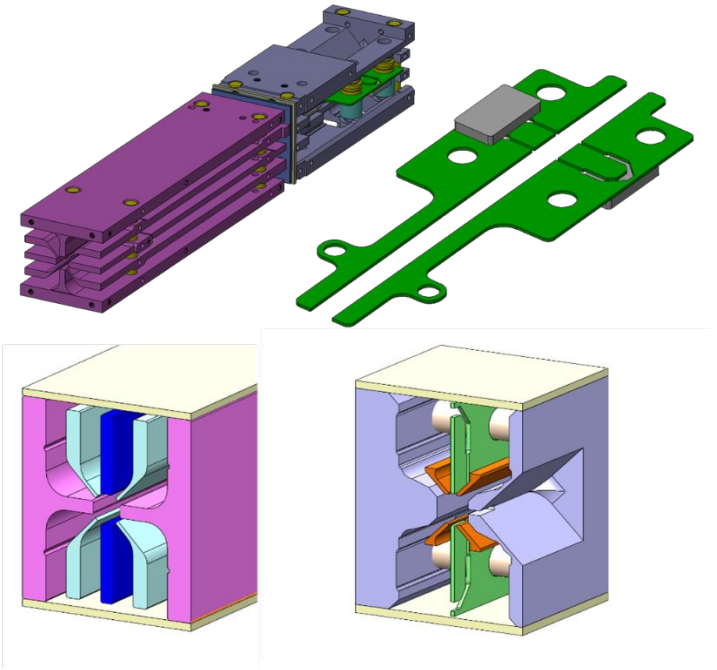

Figure S2. Improved design with electrodes glued to rods, and simplified auxiliary DC electrode structure.

Carbonic Anhydrase Intact MS

In addition to myoglobin, carbonic anhydrase was also observed and a 100-shot average spectrum is shown in Figure S3. The envelopes are isotopically resolved, and although the level of scatter is greater than for the lighter myoglobin protein spectrum, necessitating greater averaging, there may still be room for further optimization with better settings signal processing (binning) and device pressure and extraction conditions. For proteins that are so large that isotopic resolution is not achievable, it may be preferable to measure at lower resolution with a shorter ion track setting, such as when the prism deflector is set to pass ions back to the detector after only a single oscillation. Additionally, MS/MS analysis is possible, and Figure S4 shows an MS/MS spectrum of the m/z 854.7 envelope. 2.5-second-long MS/MS acquisitions were made in the Astral and Orbitrap analyzers and searched via ProSight. The Orbitrap analyzer-based search found 65 matching fragments, with 25% Residue Cleavages. The Astral analyzer-based search found 79 matching fragments and 28% Residue Cleavages, a modest improvement.

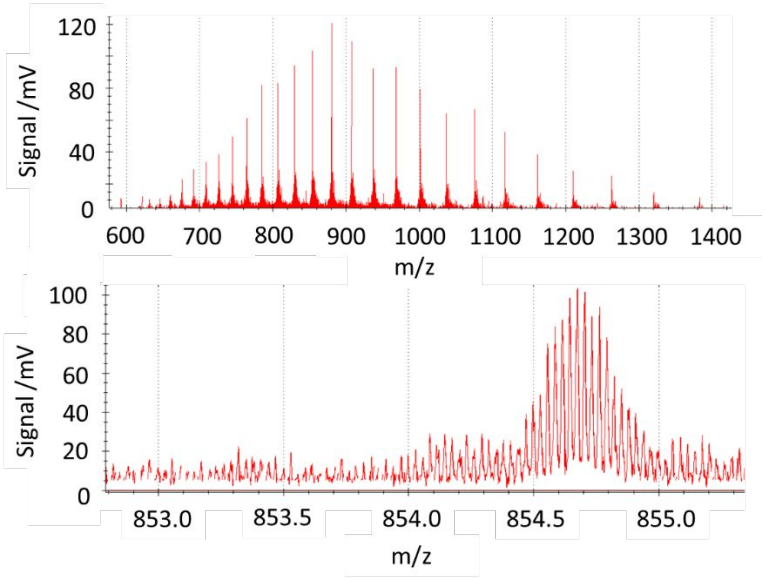

Figure S3. 100x averaged carbonic anhydrase mass spectrum, both panoramic and zoomed in on a single envelope.

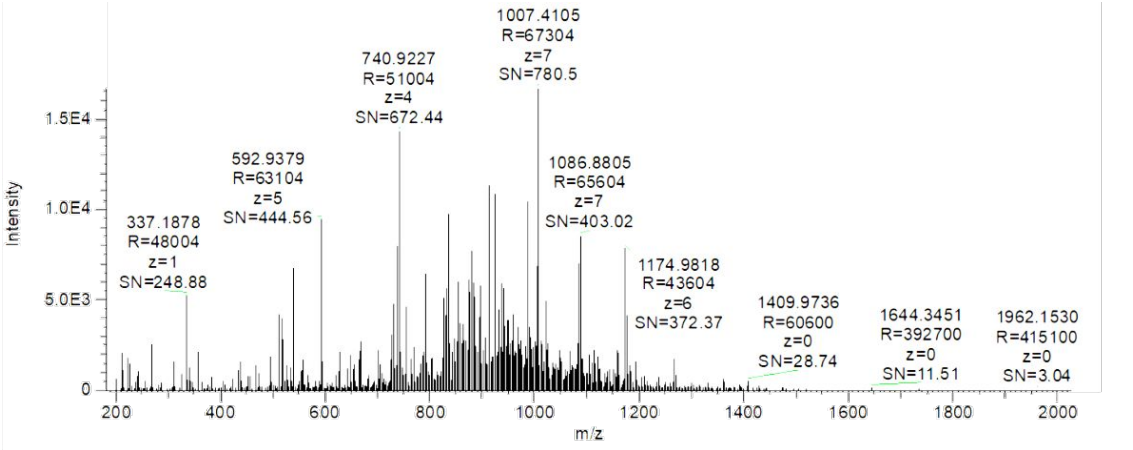

Figure S4. Carbonic Anhydrase m/z 854.7 MS/MS spectrum.

DC Electrode Trapping Losses.

An early observation was that stronger DC potentials of the auxiliary DC electrodes could remove high m/z ions from the mass spectrum, and that the trapping via the negative inner electrode suffered a much poorer mass range than a similar voltage applied to the positive outer electrode. Figure S5 shows a comparison of Flexmix mass spectra with 5V applied to each during the 4KV lift stage, with a stark loss of higher m/z ultramark peaks in negative trapping mode. The RF dependency of this high m/z loss clearly implied a weaker or perturbed radial pseudopotential well, which becomes proportionally weaker as m/z increases.

In RF trapping theory[S1], the pseudopotential well depth ψ for a linear ion trap relates to the RF amplitude V and the Matthieu trapping parameter q:

$$\psi = \frac{Vq}{4}$$

Where q is itself a function of RF amplitude V, frequency f, inscribed radius r_0, mass m and charge z.

$$q = \frac{4zV}{mr_0{}^2(2\pi f)^2}$$

MASIM3D incorporates a feature for calculation of pseudopotentials, in addition to direct potentials from static fields, which may be summed together to return a total potential. Figure S5 shows a comparison of axial and radial total potential functions around the center of the trapping region, for various applied voltages to the positive or negative trapping electrodes. These functions show potential wells around the trapping region, and for the axial well, which depends entirely on the DC amplitude and the proportional field penetration of the DC electrodes to the centerline, it shows a depth of a little less than 10% of the applied DC voltage, whether on the positive or negative electrode.

For the radial well, which includes RF pseudopotential and perturbation from the DC electrodes, it is apparent that the negative DC much more strongly flattens out the RF pseudopotential than the positive DC, at least around the center point. The reason for this is that the negative DC electrodes were positioned at the axial center point of the trapping region, whilst the positive electrodes were positioned at the periphery, so inevitably they would more strongly perturb the center. That the positive trapping electrode features a reduced RF perturbation in the ion accumulation region is an important advantage of their design, and consequently the use of the negative trapping pin was in later experiments generally avoided.

This ability of the auxiliary trapping electrodes to pull or push ions out of the radial trapping well is a limitation of the technology, at least compared to a segmented structure, that must be worked around to maximise mass range and ion capacity.

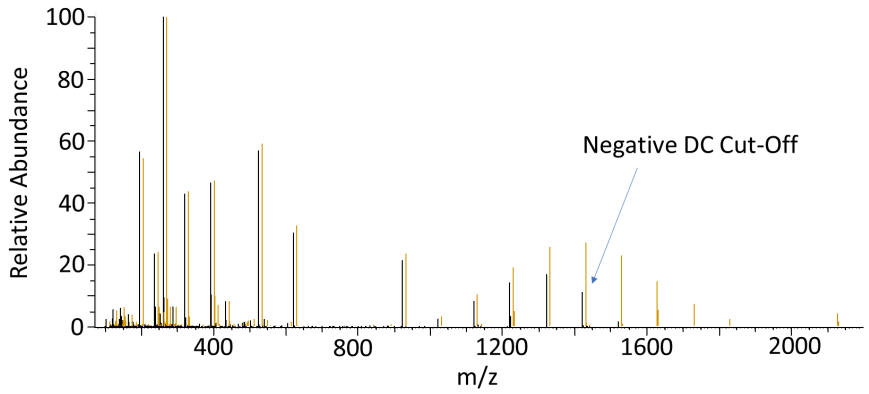

Figure S5. Superimposed FlexMix mass spectra in which axial trapping was made by -5V on inner DC electrode (black) or +5V on outer DC electrode (yellow).

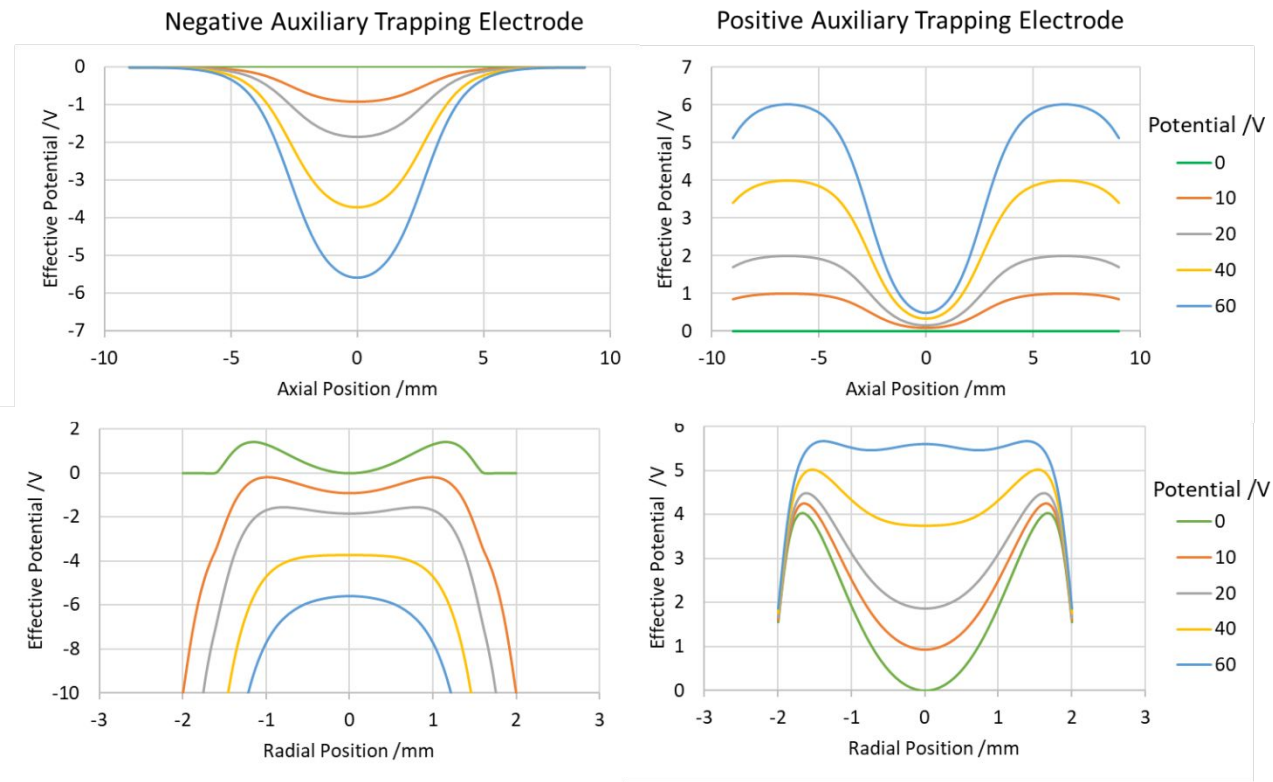

Figure S6. Axial and radial total DC+RF potential wells for m/z 1522 ion, 1000V 4.5MHz RF amplitude and various positive and negative trapping electrode potentials.

Practical quantitation of the influence of auxiliary electrodes upon the RF trapping was made by scanning the relevant auxiliary electrode DC at each ion handling stage (Injection, transfer between HP and LP regions, and during 4KV lift prior to extraction, at various RF amplitudes and monitoring 50% cut-off points for different m/z ions. Figure S7 shows the raw result of one such DC scan, as well as the linear relationship between the DC voltage cut-off point and theoretical pseudopotential well depth. Such a relationship is to be expected if the RF pseudopotential is perturbed by a proportion of the auxiliary DC.

Figure S8 then shows the ratio of this cut off point to pseudopotential well depth, averaged for several RF levels, and differentiated by mass for each stage of trap operation. During ion injection the HP region DC electrode removes ions when its DC voltage is ~3.7x the RF trapping well, but this ratio increases to ~8x during transfer of ions to the LP region. Similarly, the LP regions positive DC electrode only needs 3x the RF trapping well depth to remove ions during transfer, but this rises to 9x during 4KV lift and extraction. The reason is that both electrodes physically intrude most into the ion channel at the entrance to their respective regions, and so the field penetration is much stronger there, and ions are easily removed when they cross over these regions. This ratio could be considered a practical measurement of the proportion of field penetration by these auxiliary electrodes, possibly useful to diagnose errors in construction or assembly.

It is worth commenting that the trend is never quite as mass independent as one might hope for, particularly during the 4KV lift of the LP region. Possibly this dependence results from incomplete thermalization of high m/z ions during the experiment, leaving them in a position with greater field penetration and more readily extracted.

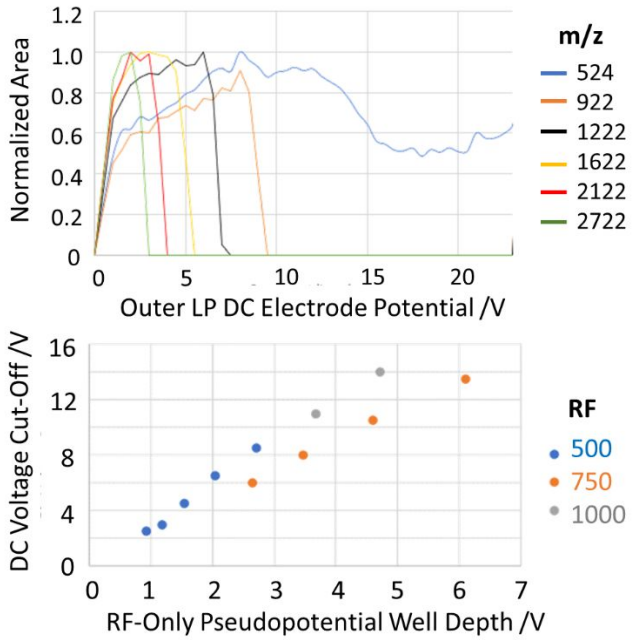

Figure S7. Top: Scan of ion signal with auxiliary DC trapping electrode potential. Bottom: Trend of DC voltage cut-off with theoretical RF pseudopotential well depth.

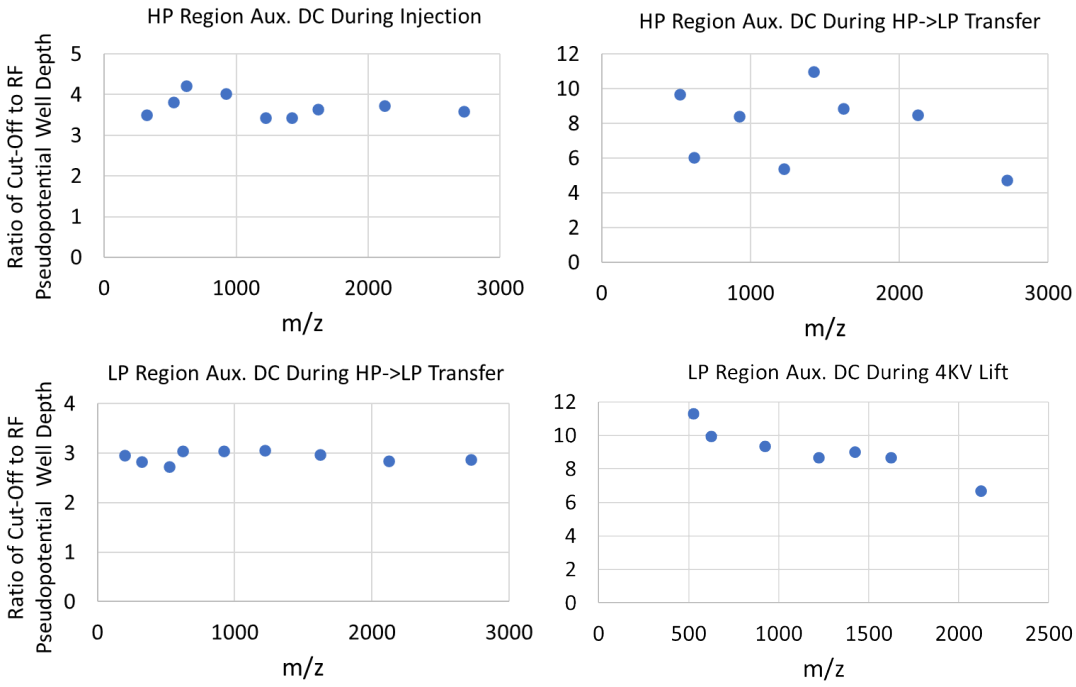

Figure S8. Ratio of auxiliary electrode DC potential required to remove ions from trap to theoretical pseudopotential well depth, for electrodes in different regions and at different stages of operation.

The implication of this experiment is that the points of greatest electrode protrusion represent weak spots in ion trapping performance and must be operated at lower DC voltage to maintain m/z range. Fortunately, the DC voltage supplies may be dynamically switched between operation stages, and this makes such optimization possible. Figure S9 shows a diagram of the Ion Processor with prominent DC electrodes and marked positions of protrusion and ion accumulation. The points of electrode protrusion are separate from the points of ion accumulation, so that low (2-3V) DC potential may be used to provide a voltage gradient to shuttle ions along, but 3x stronger potentials (9+V) may be used to clear the HP region, or to compress the ion cloud in the trapping region during the 4KV lift.

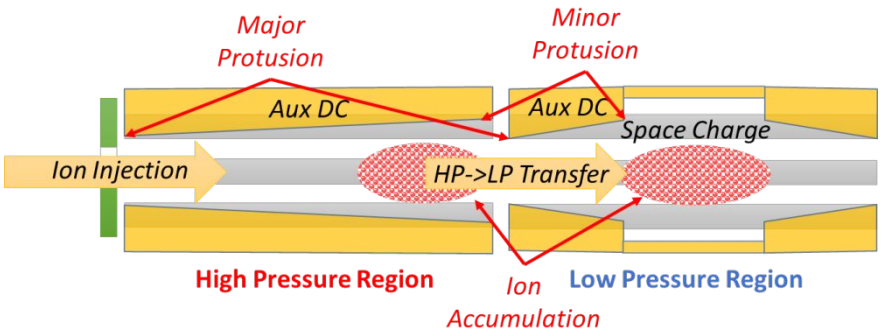

Figure S9. Schematic of the Ion Processor showing point of ion accumulation during trap operation and DC perturbation weak points.

References

[S1]Douglas, D. J., Berdnikov, A. S., & Konenkov, N. V. (2015). The effective potential for ion motion in a radio frequency quadrupole field revisited. *International Journal of Mass Spectrometry*, 377, 345-354.